The relationship between the SOI and extended tropical precipitation in simulations of future climate change

Ruth Doherty

Environmental and Societal Impacts Group, NCAR, Boulder CO, USA

Mike Hulme

Tyndall Centre for Climate Change Research, School of Environmental Sciences, University of East Anglia, Norwich, UK

Received 19 December 2001; revised 22 February 2002; accepted 22 February 2002; published 30 May 2002.

[1] The Southern Oscillation Index (SOI), its relationship with precipitation, and how greenhouse gas-induced changes in climate may modify these relationships has been examined in 12 coupled atmosphere-ocean Global Climate Model (GCM) experiments. The model SOI series predominantly show a tendency towards more positive (La Niña-like) SOI values as climate warms, but opposing trends with regard to changes in its interannual variability. EOF analyses of the dominant mode of precipitation reveals that most models display the main observed features of tropical precipitation related to ENSO. Only modest changes in the modelled EOF1 coefficient fields between the simulated periods 1900–1949 and 2050–2099 are found. The model EOF1 amplitude series, in general, correlate highly with the model SOI series for the historic 1900–1949 period. For the future 2050–2099 period, however, this correlation decreases in a number of the simulations, due either to a shift in the centres of ENSO action or to an overall weaker SOI signal. *INDEX TERMS:* 3354 Meteorology and Atmospheric Dynamics: Precipitation (1854); 3339 Ocean/atmosphere interactions (0312, 4504); 3309 Climatology (1620); 1620 Global Change: Climate dynamics (3309)

1. Introduction

[2] The El Niño Southern Oscillation (ENSO) is the dominant mode of variability in tropical precipitation on interannual timescales. *Ropelewski and Halpert* [1989] identified 15 regions of the globe, including the tropical Pacific, Indonesia and Australia, which have consistent—although opposite in sign—observed precipitation relationships for both the warm/low ENSO and the cold/high La Niña phase of the Southern Oscillation. *Dai and Wigley* [2000] found that the first EOF of global annual observed precipitation identified these core and several other regions. A relationship between tropical precipitation variability and the SOI has also been reported in studies performed with atmospheric GCMs driven by observed sea-surface temperatures (SSTs) [*Smith and Ropelewski*, 1997; *Moron et al.*, 1998].

[3] Several analyses of coupled GCM control simulations have shown the SOI and tropical SSTs averaged over the Niño-3 region (150°W–90°W, 5°S–5°N)—hereafter Niño3 SSTs—to be strongly correlated [*Tett*, 1995; *Roeckner et al.*, 1996], and therefore in agreement with observations. A number of coupled atmosphere-ocean model experiments have been examined for changes in Niño3 SSTs between present-day and future globally-warmed conditions [*Meehl et al.*, 1993; *Tett*, 1995; *Knutson et al.*, 1997; *Timmermann et al.*, 1999a, 1999b; *Collins*, 2000a, 2000b]. These model studies have given mixed results concerning changes in SST variability under greenhouse-gas increases.

0094-8276/02/2001GL014601$05.00

[4] We address a number of questions in this paper. Are simulated changes in SOI variability in coupled GCMs similar to the changes in SST variability reported above? Do coupled models predict robust SOI-precipitation relationships over the tropics similar to those observed? How does this relationship change as climate warms in the future? We investigate these questions using results from 12 coupled atmosphere-ocean GCM experiments.

2. Data and Methods

[5] Data were obtained from 12 coupled ocean-atmosphere GCM experiments held at the IPCC Data Distribution Centre (http://ipcc-ddc.cru.uea.ac.uk/dkrz/dkrz_index.html). The GCM experiments selected (Table 1) have been run with historical atmospheric CO_2 concentrations up to 1990 and a 1% per annum increase in CO_2 concentration thereafter. Greenhouse-gas only forced experiments were chosen wherever possible. The period of the simulations varied, although typically they covered the period 1860–2099. Equivalent GCM control or unforced experiments were also used to aid with statistical analyses. The data from all these simulations were gridded onto a common 3.75° × 2.5° grid.

[6] The observed SOI series (P. D. Jones, Climatic Research Unit 2001; updated from *Ropelewski and Jones* [1987]; http://www.cru.uea.ac.uk/cru/data/soi.htm) for 1866 to 2001, and the extended tropical land and ocean precipitation data-series for 1974–1994 [*Doherty et al.*, 1999] were used for model evaluation purposes. The latter is a blended gridded data-set using rain-gauge measurements over land and OLR-derived precipitation estimates over the oceans. Missing land data were not infilled with OLR measurements to maintain integrity of the gauge-measured land precipitation. Following the method *Ropelewski and Jones* [1987] used to create the observed SOI series, monthly model SOI series normalised with respect to 1951–1980 were constructed using mean sea-level pressure for the GCM grid boxes covering Tahiti (17.5S, 149.5W) and Darwin (12.5S, 130.9E). Annual average observed and model series were then formed for the period June (0) to May (+1); this period was chosen to best capture the ENSO cycle. EOF analyses, using the correlation matrix, were performed to calculate the dominant EOF1 of observed and model annual June (0)–May (+1) precipitation over the region 30°N–30°S. To investigate possible changes in future spatial and temporal characteristics of EOF1 precipitation, EOF analyses was performed on two separate 50-year time periods: 1900–1949 hereafter the "historic" period and 2050–2099 hereafter the "future" period. As the ECHAM3, GFDL-R15 and DOE-PCM experiments were shorter, slightly different periods had to be selected for EOF analyses in these models (Table 1). The observed and modelled SOI and EOF1 precipitation series were inter-compared and the historic and future relationship between the SOI and EOF1 precipitation amplitude time series examined. Monte Carlo analyses using results from the control experiments were performed, in

Table 1. Details and results from the GCM Experiments (Columns 1–3)

June (0)–May (+1) EOF1 Precipitation	"Historic" and "Future" Periods	Resolution[a] Atmosphere Ocean	% Variance Explained "Historic"	% Variance Explained "Future"	Correlation "Historic" and "Future" EOF1 Patterns	Correlation SOI and EOF1 Precipitation "Historic"	Correlation SOI and EOF1 Precipitation "Future"
Obs 1974–94:			34.7			−0.89	
HadCM2-gg1	1900–49;	2.5 × 3.75 L19	28.2	25.8	0.72	−0.90	−0.23
HadCM2-gg2	2050–99	2.5 × 3.75 L20	24.6	29.3	0.72	−0.88	−0.24
HadCM2-gg3			24.5	22.8	0.74	−0.90	−0.27
HadCM2-gg4			25.1	29.3	0.73	−0.84	−0.41
HadCM3	1900–49;	2.5 × 3.75 L19	21.3	22.6	0.79	−0.80	−0.81
	2050–99	1.25 × 1.25 L20					
ECHAM3/LSG	1900–49;	T21 (5.6 × 5.6) L19	11.7	10.7	0.59	−0.71	−0.51
	2035–84	4.0 × 4.0 L11					
ECHAM4/OPYC	1900–49;	T42 (2.8 × 2.8) L19	24.6	21.1	0.80	−0.81	−0.29
	2050–99	2.8 × 2.8 L11					
CGCM1	1900–49;	T32 (3.8 × 3.8) L10	15.1	13.8	0.45	−0.91	−0.80
	2050–99	1.8 × 1.8 L29					
CCSR/NIES	1900–49;	T21 (5.6 × 5.6) L20	22.6	14.3	0.79	−0.75	−0.41
	2050–99	2.8 × 2.8 L17					
CSIRO-Mk2	1900–49;	R21 (3.2 × 5.6) L9	11.4	13.7	0.82	−0.65	−0.73
	2050–99	3.2 × 5.6 L21					
GFDL-R15-a	1961–2000;	R15 (4.5 × 7.5) L9	6.2	6.5	0.57	−0.75	−0.82
	2017–56	4.5 × 3.7 L12					
DOE-PCM	1961–2000;	T42 (2.8 × 2.8) L18	10.8	12.6	0.76	−0.63	−0.67
	2060–99	0.67 × 0.67 L32					

Details of GCM experiments (Columns 1–3). Further details of these model experiments, including references and modelling centre, can be found in Table 9.1 of Chapter 9 [*Cubasch and Meehl*, 2001] of the IPCC WG1 Third Assessment Report. Percentage variance explained by (Columns 4–5) and spatial pattern correlations (Column 6) between, EOF1 historic and future precipitation coefficients fields. The relationship between the SOI and EOF1 precipitation amplitude series (Columns 7 and 8). All model experiments use historical atmospheric concentrations of CO_2 until 1990 then 1% increase per year thereafter (GG); the DOE–PCM experiment also includes the direct effect of sulphate aerosols (GS since GG was not available). Only the HADCM3 and DOE-PCM models do not employ flux corrections.

[a] All the GCM experiment data obtained from the IPCC Data Distribution Centre were regridded onto a common 2.5° × 3.75° grid.

conjunction with standard statistical tests, to assess statistical significance.

3. SOI Series

[7] The observed and modelled annual June(0) – May(+1) SOI series are shown in Figure 1, along with the standard deviation values for each series. For HadCM3, ECHAM4, and CGCM1, the standard deviations were similar to or higher than the observed series, whilst for the other model SOI series values were lower. ECHAM4 shows a marked increase in SOI values from the 2060s onwards, reflecting a shift towards more La Niña-like conditions (Figure 1). The SOI series derived from the CCSR/NIES and HadCM3 models also exhibit large positive trends. In contrast, CGCM1 exhibits a negative (El Niño-like) trend from the 1990s onwards. All four of these trends are significant at the 99% level. Furthermore, through re-sampling of trends in the model control experiments, we found the slope values in these climate change experiments to be greater than the p(99) value in the distribution of values formed from the respective control experiments. Thus, we can be confident that these three positive and one negative trends are greater than those that would occur due to internal model variability. The HadCM2-gg3, gg4 and CSIRO experiments also showed positive trends in SOI, significant at the 95% or 99% level and which exceeded the p(90) and p(95) values of the re-sampled distributions from their control experiments. Of the five remaining model experiments showing non-significant trends, only the DOE-PCM model showed a tendency towards more negative SOI values.

[8] We conclude that, overall, as climate warms the SOI index exhibits more of a tendency towards higher positive future values (a La Niña-like state) than towards higher negative values. This conflicts with the results of *Timmermann et al.* [1999a, 1999b], and *Cai and Whetton* [2000] which show a future pattern of Pacific SST warming and hence a tendency towards a more El Niño-like state as climate warms. The warming trend exhibited by the Niño-3 SSTs is not therefore reflected in the behaviour of the SOI.

[9] Examining historic and future variability of the de-trended model SOI series, we find significant (at the 95% level) changes in the variances. There is increased variability in HadCM3 and ECHAM4 and decreased variability in HadCM2-gg3, CGCM1 and CCSR/NIES, with the remaining experiments showing little

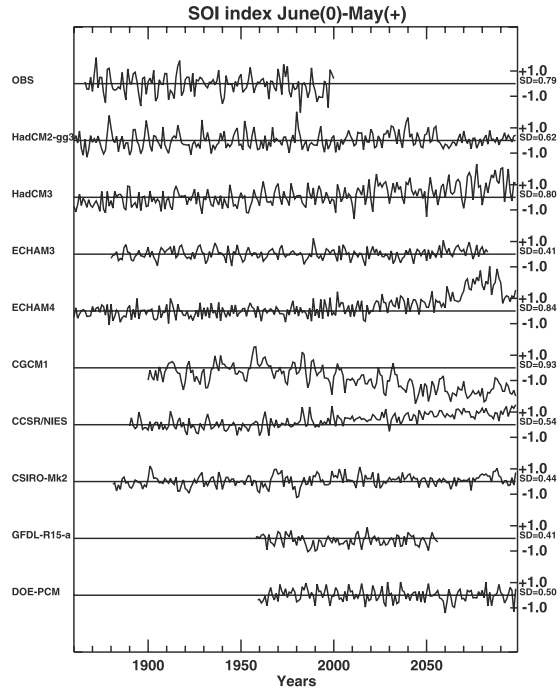

Figure 1. Annual SOI series observed and constructed for different GCMs. The different experiment periods are given in Table fc1. For HadCM2 only greenhouse-gas member gg3 is

change. Re-sampled distributions of 50-year standard deviation values were again formed from the respective control experiments. These showed the SOI standard deviations for the future period for HadCM3 and ECHAM4 to be higher than the re-sampled p(99) value, and to be lower for HadCM2-gg3 (p(5)), CGCM1 (p(5)) and CCSR/NIES (p(1)). Interannual variability also increased towards the end of the Niño3 SST series in the four HadCM2 and the ECHAM4 greenhouse-gas experiments [*Collins*, 2000a; *Timmermann et al.*, 1999b], thus in these model experiments climate warming affected the amplitude of both the SOI and SST series.

[10] Frequency distributions (not shown) of the de-trended SOI series were formed for the two periods. For ECHAM4, greater numbers of positive anomalies >1.0 (La Niña episodes) were found for the future period compared to the historic, with the two distributions significantly different from each other at the 95% level. This agrees with the result of *Timmermann et al.* [1999b] who showed the distribution of Niño3 SST anomalies in ECHAM4 to be skewed towards a higher frequency of La Niña events in the latter half of the series. HadCM3 showed an increase and CCSR/NIES a decrease (the latter significant at the 7% level) in both tails of the distribution in the future period. The p-values for the upper (p(99)) and lower (p(1)) tails for HadCM3 and the upper tail (p(99)) for ECHAM4 of the distributions in the future period were higher than the respective p-values for the tails of the distributions formed from the re-sampled control series. The SOI frequency distributions for the two periods in the other model experiments are similar.

4. EOF1 ENSO-like Precipitation Patterns

[11] The EOF1 annual June(0)–May(+1) precipitation coefficients field for the observed series (1974–1994) is depicted in Figure 2a. The EOF coefficients show a strong positive pattern over the Central and Eastern Equatorial Pacific extending southeastwards in the South Pacific. Strong negative patterns are located over the western Equatorial Pacific and Indonesia extending northeast into the North Central Pacific and southeastwards over Australia and the South Pacific. A negative pattern stretches from northeast South America across the Atlantic to Africa, as noted by *Dai and Wigley* [2000]. A negative pattern also is seen over southern Africa. The amplitude of observed EOF1 precipitation shows peak increases in known ENSO years (1982, 1986, 1991; Figure 2a). The first EOF explains 35% of the variance in observed tropical precipitation (Table 1, column 4). This variance explained for the first EOF of precipitation over the entire tropics is higher than in other studies where land-only datasets have been analysed.

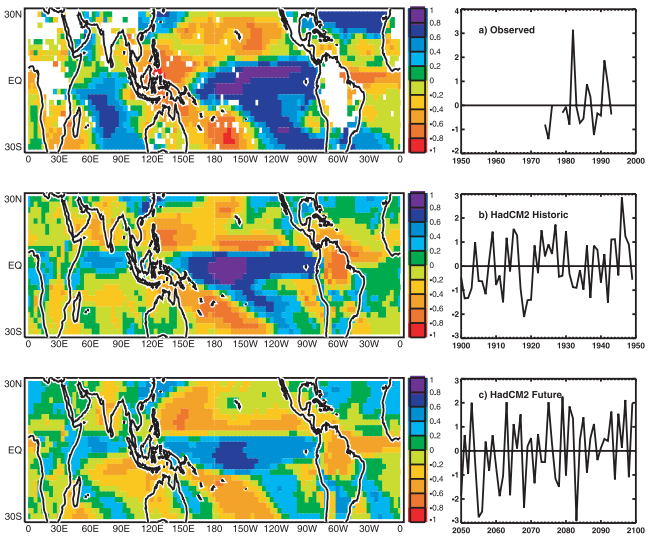

Figure 2. EOF1 precipitation coefficients field and amplitude time series for: (a) observed for 1974–1994 and HadCM2-greenhouse gas member (gg2), (b) historic (1900–1949), and (c) future (2050–2099) periods. N.B. The years 1977 and 1978 are not included in the observed series due to missing OLR satellite measurements over this period.

[12] The EOF1 coefficient fields and amplitude time-series for HadCM2-gg2 for the historic and future periods are shown in Figures 2b and 2c, respectively. The GCM-derived EOF1 precipitation fields from the greenhouse-gas experiments show some variation across the GCMs. For both periods, the majority of the models reproduce the strong ENSO-like patterns of positive and negative coefficients across the Pacific and Indian oceans described above, but with the following notable exceptions. In both periods, CGCM1 and GFDL-R15-a do not show the strong positive meridional pattern across the East and Central Pacific, and CGCM1 and CSIRO_Mk2 have the extension of negative pattern centred over the West Pacific/Indonesia northwards instead of northeastwards into the Central Pacific. The first EOF of tropical precipitation in HadCM2, HadCM3, ECHAM4 and CCSR/NIES accounts for more than 20% of the total variance of precipitation in the historical period (Table 1, column 4). Spatial pattern correlation coefficient values between the observed and the GCM historical EOF1 fields are highest for HadCM2, HadCM3 and ECHAM4 (0.53–0.58).

[13] Most models show only modest changes in spatial patterns from the historical to future periods (Table 1, column 6). The variance explained by the first EOF of precipitation also shows little change for this future period (Table 1, column 5). For both periods, the first EOF is well separated [see *North et al.*, 1982] from the second EOF in all models (except ECHAM3 in the future period), with the second EOF only explaining between 3–9% of the variance. The patterns of EOF1 coefficients show the largest change for CGCM1, in which a southeastward shift occurs in the overall pattern in the future period.

[14] To assess whether the changes in EOF patterns between the two periods were solely a function of internal model variability, for each model control experiment we calculated a matrix of pattern correlations for the first EOF of precipitation for 50-year periods at approximately 20-year intervals. For ECHAM4, CGCM1 and DOE-PCM the correlation coefficients between the historic and future periods for the climate change integrations are lower (especially for CGCM1) than any of the values in the matrix of correlation coefficients in the respective control experiments. The changes in EOF patterns in these three experiments are therefore greater than would be expected from internal model variability.

[15] For the future period, the HadCM2 (except gg4), ECHAM4 and CCSR/NIES EOF1 coefficients fields correlate less well with the observed EOF1 field, whilst the other seven model fields correlate better. Correlation coefficients amongst the different models for the historic and future periods were also calculated (not shown). Intra-model EOF1 precipitation fields show a high level of similarity, with the four HadCM2 experiments all correlating with each other at ~0.9, in both periods. The highest inter-model correlation coefficients have values of the same order as, or greater than, model-observed values– in the range 0.5 to 0.65.

5. SOI-Precipitation Relationships

[16] Correlation coefficients between the June(0)–May(+1) annual EOF1 precipitation amplitude and SOI time series (both de-trended) for the observed and model historical and future periods are given in Table 1 (columns 7 and 8). The EOF1 time series of observed precipitation has a strong inverse correlation of −0.89 (increasing to −0.94 with a 2–3 month lag) with the observed SOI series. *Dai and Wigley* [2000] found a correlation of −0.71 between the first EOF of annual precipitation and Darwin sea-level pressure, increasing to −0.76 for a two-month lag.

[17] In all the models over the historic period, the EOF1 precipitation series correlate above −0.6 with the SOI series (Table 1,

column 7). Furthermore, HadCM2 (−0.85 to −0.90), HadCM3 (−0.84), ECHAM4 (−0.83) and CGCM1 (−0.89) produce highly significant correlations (at the 99.9% level), with values that are in close agreement with the observed result above for zero lag.

[18] In the future period, correlations between −0.7 and −0.8 are obtained for HadCM3, CGCM1, CSIRO-Mk2, GFDL-R15-a and DOE-PCM (Table 1, column 8). For these models (except CGCM1), correlations are higher in this future period than in the historic period. HadCM2, ECHAM4 and CGCM1, however, which show high agreement with observations over the historic period, as well as ECHAM3 and CCSR/NIES, show decreases in their correlation coefficients in the future period. In the case of HadCM2, ECHAM4 and CCSR/NIES, the relationship between SOI and EOF1 precipitation is greatly weakened (no longer significant at the 95% level). These correlation coefficients were also compared to correlation coefficients calculated by re-sampling control experiments. The values for the future period are lower than the p(1) re-sampled values for ECHAM4 and CCSR/NIES, and the p(5) values for HadCM2 and CGCM1. The changes in the relationship between the SOI and the tropical Pacific precipitation EOF1 amplitude series in the future period for HadCM2, ECHAM4, CGCM1 and CCSR/NIES therefore lie outside the range expected due to internal model variability.

[19] To investigate why this SOI/EOF1 precipitation relationship weakened in some model experiments, we examined the correlation between the spatial pressure fields and EOF1 precipitation amplitude series. For HadCM2 and ECHAM4, the centres of action of pressure-ENSO-precipitation related activity shift eastwards in the future period. This means that Tahiti, which had the opposite sign of correlation coefficient to Darwin in the historic period, now lies at the edge of the same center of action as Darwin and therefore has the same sign correlation coefficient. CCSR/NIES, ECHAM3 and CGCM1 do not show such a phase shift in the future, but do show a weaker pattern over Tahiti and Darwin. The other models show slightly stronger patterns in both periods. Thus, there are changes in the spatial structure of ENSO-related pressure variability under conditions of climate warming may require a broader, or more refined, definition of the SOI index. Examining the spatial relationship between tropical precipitation and the SOI, we find a weaker pattern for HadCM2, ECHAM3, ECHAM4, CGCM1 and CCSR/NIES and a stronger pattern for HadCM3, CSIRO-Mk2, GFDL-R15-a and DOE-PCM in the future period.

6. Conclusions

[20] Examination of 12 climate change experiments conducted using coupled atmosphere-ocean models reveals an overall tendency towards more positive (La Niña-like) SOI values. This result conflicts with a tendency towards a more El Niño-like mean state found in earlier studies that examined Niño-3 SST indices in (some of) these same transient climate change experiments. These two ENSO indices reflect behaviour in different geographical regions of the Pacific. Under conditions of climate warming, and consequent possible shifts in ENSO centres of action, these indices may therefore exhibit different ENSO-related behaviour. There is, however, no overall model consensus regarding future change in SOI variability, with some model experiments showing an increase and others a decrease in SOI amplitude.

[21] The EOF1 precipitation coefficient fields produced for each GCM for a historic and future period in general depict adequately the main observed features of precipitation related to ENSO over the Pacific and Indian Ocean regions. Most models also reproduce the observed inverse relationship between the SOI and the EOF1 precipitation amplitude series for the historic period. Correlations between model-simulated SOI and EOF1 precipitation in HadCM2, HadCM3, ECHAM4 and CGCM1 agree closely with observations. Although the relationship between the SOI and EOF1 precipitation amplitudes remains fairly high in the future for a number of models, this relationship weakens greatly for others. This is notable for HadCM2 and ECHAM4 and, to a lesser extent, for ECHAM3 and CCSR/NIES. For HadCM2 and ECHAM4, a shift in centres of action of ENSO-related pressure occurs for the future period such that there is a lesser pressure gradient between Tahiti and Darwin. Further investigation into the use, and possible refinement, of the SOI Index as a robust measure of ENSO variability under conditions of climate warming is warranted.

[22] **Acknowledgments.** This work has been supported by the UK DETR under Contract Number EPG 1/1/85. The authors obtained model data from the IPCC DDC and through the Climate Impacts LINK Project and Tim Osborn at the University of East Anglia (UEA). The observed SOI data were obtained from Phil Jones (UEA). We especially thank Rick Katz (NCAR), Linda Mearns (NCAR) and Tim Osborn for statistical advice. We also acknowledge three anonymous reviewers for a number of helpful comments.

References

Cai, W., and P. H. Whetton, Evidence for a time-varying pattern of greenhouse warming in the Pacific Ocean, *Geophys. Res. Lett.*, *27*, 2577–2580, 2000.

Collins, M., The El Niño-southern Oscillation in the second Hadley Centre coupled model and its response to Greenhouse warming, *J. Climate*, *13*, 1299–1312, 2000a.

Collins, M., Understanding uncertainties in the response of ENSO to greenhouse warming, *Geophys. Res. Lett.*, *27*, 3509–3512, 2000b.

Cubasch, U. and G. Meehl, Chapter 9: Projections of future climate change, in *IPCC WG1 third assessment report Climate Change 2001: The scientific basis*, edited by J. Houghton et al., 524–582, 2001.

Dai, A., and T. M. L. Wigley, Global patterns of ENSO-induced precipitation, *Geophys. Res. Lett*, *27*, 1283–1286, 2000.

Doherty, R. M., M. Hulme, and C. G. Jones, A gridded reconstruction of land and ocean precipitation for the extended tropics from 1974 to 1994, *Int. J. Climatol.*, *19*, 119–142, 1999.

Knutson, T. R., S. Manabe, and D. Gu, Simulated ENSO in a global coupled ocean-atmosphere model: Multidecadal amplitude modulation and CO_2 sensitivity, *J. Climate*, *10*, 42–63, 1997.

Meehl, G. A., G. W. Branstator, and W. M. Washington, Tropical Pacific interannual variability and CO2 climate change, *J. Climate*, *6*, 42–63, 1993.

Moron, V., A. Navarra, M. N. Ward, and E. Roeckner, Skill and reproducibility of seasonal rainfall patterns in the tropics in ECHAM-4 GCM simulations with prescribed SST, *Climate Dynamics*, *14*, 83–100, 1998.

North, G. R., T. L. Bell, R. F. Cahalan, and F. J. Moeng, Sampling errors in the estimation of empirical orthogonal functions, *Mon. Wea. Rev.*, *110*, 699–706, 1982.

Roeckner, E., J. M. Oberhuber, A. Bacher, M. Christoph, and I. Kirchner, ENSO variability and atmospheric response in a global coupled atmosphere-ocean GCM, *Climate Dynamics*, *12*, 737–754, 1996.

Ropelewski, C. F., and P. D. Jones, An extension of the Tahiti-Darwin Southern Oscillation Index, *Mon. Wea. Rev.*, *115*, 2161–2165, 1987.

Ropelewski, C. F., and M. S. Halpert, Precipitation patterns associated with the high index phase of the Southern Oscillation, *J. Climate*, *2*, 268–284, 1989.

Smith, T. M., and C. F. Ropelewski, Quantifying Southern Oscillation-precipitation relationships from an atmospheric GCM, *J. Climate*, *10*, 2277–2284, 1997.

Tett, S., Simulation of El Niño-Southern Oscillation-like variability in a global AOGCM and its response to CO_2 increase, *J. Climate*, *8*, 1473–1502, 1995.

Timmermann, A., M. Latif, A. Grötzner, and R. Voss, Modes of climate variability as simulated by a coupled general circulation model. Part 1: ENSO-like climate variability and its low frequency modulation, *Climate Dynamics*, *15*, 605–618, 1999a.

Timmermann, A., J. Oberhuber, A. Bacher, M. Esch, M. Latif, and E. Roeckner, Increased El Niño frequency in a climate model forced by future greenhouse gas warming, *Nature*, *398*, 694–696, 1999b.

R. Doherty, Environmental and Societal Impacts Group, NCAR, P.O. Box 3000, Boulder, CO 80305, USA. (rdoherty@ucar.edu)

M. Hulme, Tyndall Centre for Climate Change Research, School of Environmental Sciences, University of East Anglia, Norwich, NR4 7TJ, UK. (m.hulme@uea.ac.uk)